Micropillar compression of LiF [1 1 1] single crystals: Effect of size, ion irradiation and misorientation

R. Soler [a], J.M. Molina-Aldareguia [a,*], J. Segurado [a,b], J. Llorca [a,b], R.I. Merino [c], V.M. Orera [c]

A B S T R A C T

The mechanical response under compression of LiF single crystal micropillars oriented in the [1 1 1] direction was studied. Micropillars of different diameter (in the range 1–5 μm) were obtained by etching the matrix in directionally-solidified NaCl–LiF and KCl–LiF eutectic compounds. Selected micropillars were exposed to high-energy Ga^+ ions to ascertain the effect of ion irradiation on the mechanical response. Ion irradiation led to an increase of approximately 30% in the yield strength and the maximum compressive strength but no effect of the micropillar diameter on flow stress was found in either the as-grown or the ion irradiated pillars. The dominant deformation micromechanisms were analyzed by means of crystal plasticity finite element simulations of the compression test, which explained the strong effect of micropillar misorientation on the mechanical response. Finally, the lack of size effect on the flow stress was discussed to the light of previous studies in LiF and other materials which show high lattice resistance to dislocation motion.

1. Introduction

Micropillar compression tests have become popular in recent years to study the effect of specimen size (in the range of micron and sub-micron pillar diameter) on the mechanical properties of single-crystals in the absence of strain gradients. The first studies were carried out in Ni and Au, face-centered-cubic (fcc) metals (Uchic et al., 2004; Greer et al., 2005; Volkert and Lilleodden, 2006), and reported a strong increase in the flow stress as the micropillar diameter decreased below ≈10 μm. The flow stress was generally found to scale with an inverse power of specimen diameter, $\sigma_y \propto d^{-n}$, with $n \sim 0.6$. The origin of this behavior has been studied in detail and summarized in several recent reviews by Uchic et al. (2009), Dehm (2009) and Greer and De Hosson (2011). The mechanisms responsible for the increase in flow strength for single crystal micropillars in the micrometer range appeared to be the truncation of double-arm Frank–Read sources by the free surfaces (Parthasarathy et al., 2007; Rao et al., 2008) and the source exhaustion hardening due to the limited number of operating sources (Parthasarathy et al., 2007; Rao et al., 2008; Akarapu et al., 2010) or the exact initial dislocation network (Ngan, 2011). In the submicrometer region, higher flow stresses seemed to be controlled by the starvation of mobile dislocations as they exited the finite-size micropillar, which resulted in the nucleation of new dislocations to sustain the plastic flow (Greer et al., 2005; Greer and Nix, 2006). However, the competition between nucleation, multiplication and starvation of dislocations is still unclear, and very likely, should depend on the crystal structure as well as on the initial dislocation network.

This latter statement is supported by recent results published in the open literature. For instance, bcc Mo single crystals subjected to ion irradiation have shown more limited effects of the specimen size on the flow stress with n values in the

range 0.21–0.48 (Schneider et al., 2009a,b; Greer et al., 2008), while the size effect on the flow stress was virtually negligible in strong solids, like GaAs (Michler et al., 2007), Si (Moser et al., 2007; Korte et al., 2011) with $n \approx 0.1$ and Bulk Metallic Glasses (Jang et al., 2011). In addition, Bei et al. (2007) showed that the deformation of dislocation-free Mo pillars fabricated by directional solidification and etching (thus, non subjected to ion irradiation) was controlled by the nucleation of dislocations. They showed no size effect and that the yield stress was close to the theoretical strength, following the typical behavior of whiskers (Brenner, 1958). However, a large reduction in the yield stress was found when the micropillars were subjected to focused ion beam (FIB) irradiation (Bei et al., 2008), and this behavior was attributed to the surface defects introduced by the Ga^+ ion beam. FIB machining is well known to introduce defects on the machined micropillars but the exact nature and extent of the defects is material dependent and their effects are still the subject on strong debate. Previous studies in Cu (Kiener et al., 2007) report the formation of a Ga^+ ion implanted amorphous damage layer of several nm in depth (Kiener et al., 2007) and/or defects that result in lattice distortions (Maas et al., 2008), leading to significant changes in the deformation micromechanisms (Bei et al., 2008). Previous experiments in Ni (Shan et al., 2007) have also shown that most of the ion induced damage is driven out of Ni crystals during mechanical loading, suggesting no amorphous layer forming. In any case, the most widely accepted view in metals is that provided the micropillars are not dislocation free (like the Mo pillars of Bei et al., 2008), FIB induced damage does not strongly affect the micropillar compression behavior. This has been nicely demonstrated by Discrete Dislocation Dynamics (DDD) simulations (El-Awady et al., 2009), showing that even if strong intermetallic particles form during FIB milling, the effect can increase the strength by 25% but only to a very small window of crystal sizes (<1.0 μm).

One striking example found in the literature is the behavior observed by Nadgorny et al. (2008) in alkali halide LiF [1 0 0] micropillars machined by FIB both from dislocation-free and γ-irradiated bulk single-crystals. A very large size effect exponent n, in the range 0.7–0.8, was found, independently of the initial dislocation density of the original bulk single-crystal, suggesting a similar behavior to that observed in fcc metals (Dimiduk et al., 2010). Also remarkable was the fact that both pristine and γ-irradiated bulk single-crystals showed a very similar behavior, when the plastic deformation of LiF is known to be extremely sensitive to ion irradiation (Johnston and Gilman, 1959). LiF micropillars were fabricated by FIB milling and the size effects and flow stresses reported might be due the FIB-induced defects which dominated the deformation behavior. In addition, the plastic flow of LiF single crystals is highly anisotropic due to its crystal structure. LiF has a fcc lattice but the standard $\{1\,1\,1\}\langle 1\,1\,0\rangle$ slip system is not activated to keep neutrality of charges in the ionic Li^+ and F^- crystal. Instead, the preferred slip system belongs to the $\{1\,1\,0\}\langle 1\,1\,0\rangle$ family, that is usually referred to as the "soft" slip system. There are only six independent slip systems of this type which are not enough to accommodate an arbitrary plastic deformation. Therefore, other "hard" slip systems of the family $\{1\,0\,0\}\langle 1\,1\,0\rangle$ can be activated even though their critical resolved shear stress is much higher (of the order of twenty times) (Gilman, 1959). Plastic anisotropy and the activation of different slip systems has a strong influence in the micropillar compression tests, as shown in MgO (Korte and Clegg, 2010), a ceramic with the same crystal structure of LiF, that displays very different size effects depending on the crystal orientation and the active slip system.

To the light of these previous results, this investigation was aimed at ascertaining the effect of size, ion irradiation and crystal orientation on the behavior of LiF single crystal micropillars. Compression tests were carried out in [1 1 1] oriented LiF micropillar single-crystals using a similar approach to that pioneered by Bei et al. (2007) to fabricate the micropillars. In our case, LiF single-crystal micropillars were prepared by chemically etching the matrix of directionally solidified NaCl–LiF and/or KCl–LiF eutectics. The micropillar diameter depended on the eutectic growth rate and micropillars with diameters in the range 1–5 μm could be produced without the need of FIB milling. Selected pillars were exposed to the ion beam inside a FIB workstation to study the effect of the ion-irradiation induced defects. The results were very different from those observed in [1 0 0] LiF micropillars by Nadgorny et al. (2008). The differences can be explained in terms of the crystal structure of LiF and its crystal anisotropy, for which the dominant deformation micromechanisms were analyzed by means of crystal plasticity finite element simulations of the compression test. The effect of size, crystal orientation and FIB induced defects on the mechanical response of LiF micropillars was finally assessed.

2. Experimental procedure

2.1. Micropillar fabrication

Directionally-solidified eutectics are composites fabricated from the melt which present a fine and homogeneous microstructure. When the minority compound in the eutectic composition is below 30%, it grows in the form of fibers embedded in a matrix of the majority compound (Llorca and Orera, 2006). LiF–NaCl and LiF–KCl eutectic rods were grown by directional solidification using the Bridgman method. The eutectic composition is 71 wt% NaCl/29 wt% LiF and 91 wt% KCl/9 wt% LiF, leading to the formation under coupled growth conditions of a regular microstructure formed by LiF rods aligned parallel to the growth direction (Llorca and Orera, 2006). The LiF rods occupied 25% and 7% volume in NaCl–LiF and KCl–LiF eutectics, respectively, and were arranged in almost hexagonal pattern, as shown in Fig. 1(a). The diameter of the LiF rods was determined by the growth rate, the rod diameter increasing as the growth rate decreased. Different growth rates were selected to ensure a satisfactory alignment of the rods and diameters around 5 μm (NaCl–LiF solidified at 3 mm/h) (Orera and Larrea, 2005; Orera et al., 2005), 2.5 μm (KCl–LiF solidified at 10 mm/h) and 1 μm (KCl–LiF solidified at 50 mm/h). The fibers grew with the longitudinal axis aligned in the [1 1 1] crystallographic direction.

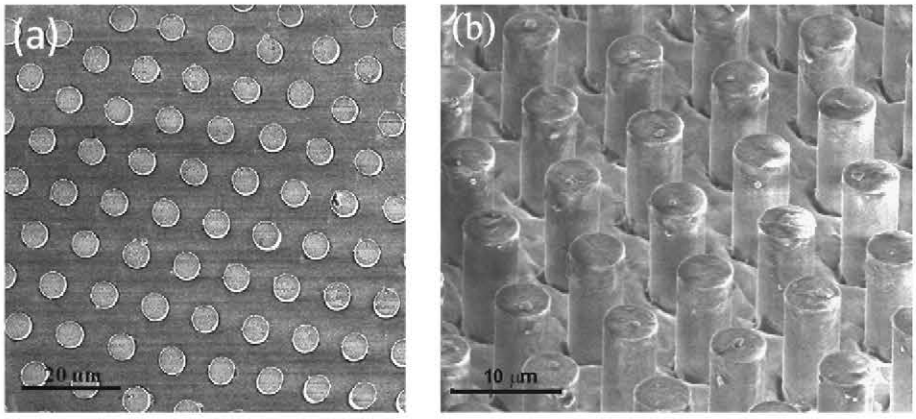

Fig. 1. (a) Cross-sectional area of a LiF–NaCl eutectic ingot, directionally solidified by the Bridgman method at 3 mm/h. The fibers, around 5 μm diameter, occupy 25% of the volume. (b) LiF–NaCl eutectic sample after matrix etching. LiF fibers are 5 μm in diameter and 10 μm in length.

The sample surface perpendicular to the growth direction was ground with 2000 grit sandpaper under dry conditions (NaCl is rapidly dissolved under any lubricated polishing), followed by polishing with 1 μm diamond powder. Surface impurities were washed-out with acetone before etching the matrix with methanol. Methanol was chosen because its low reactivity with NaCl (14.9 gr/L) and KCl (5.6 gr/L), providing a very accurate control of the etching rate. Etching times (between 2 and 10 min, depending on the fiber diameter and the matrix chemical composition) were adjusted to obtain LiF micropillars with an aspect ratio (length to diameter ratio) in the range 2:1–2.3:1. This aspect ratio is short enough to suppress buckling during micropillar compression while the effect of stress concentrations at the ends of the micropillar are minimized. The typical appearance of the LiF "forest" obtained after matrix etching is shown in Fig. 1(b).

Some LiF micropillars (as those shown in Fig. 1(b)) were further micro-machined by FIB in a FEI Helios 650 Dual Beam system, to study the effect of ion irradiation on the mechanical behavior. The Ga^+ ion accelerating voltage was 30 keV with beam currents in the range 7.7–40 pA. These currents are comparable to the values reported in the literature for micropillar fabrication using FIB (Nadgorny et al., 2008; Korte and Clegg, 2010; Östlund et al., 2011; Kiener et al., 2006; Ng and Ngan, 2008a,b,c; Uchic and Dimiduk, 2005). All pillars were imaged by Scanning Electron Microscopy (SEM) before and after ion irradiation. Fig. 2 shows images of micropillars of 1, 2.5 and 5 μm in diameter, before and after ion irradiation. The FIB'ed pillars presented tapering angles of 2–3°, as expected from the annular milling process. These values are in agreement with the results published in the literature for micropillars manufactured by FIB (Korte and Clegg, 2010; Zhang et al., 2006; Shim et al., 2009).

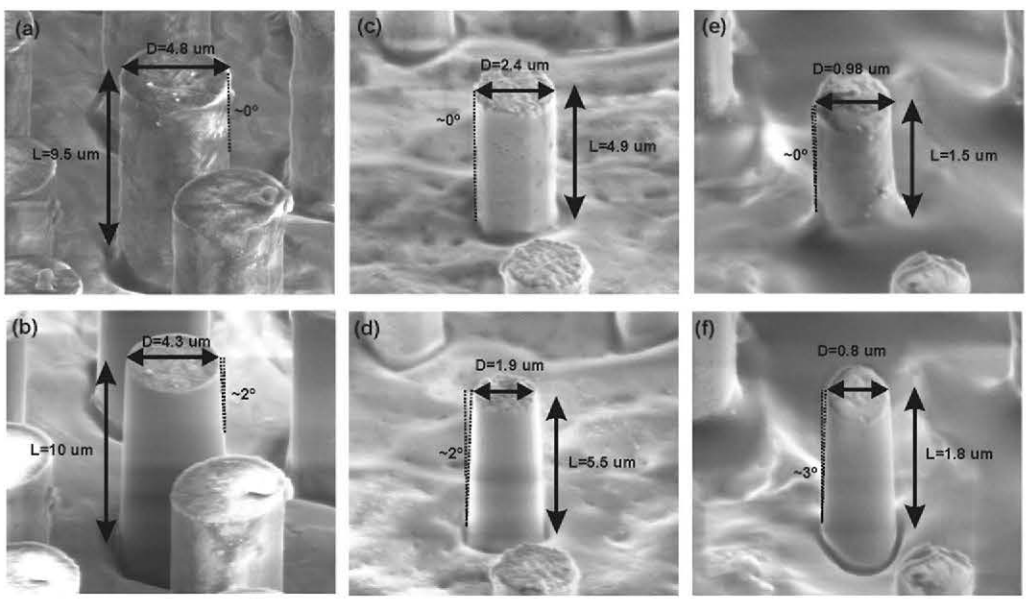

Fig. 2. SEM images of representative micropillars: (a) and (b) correspond to micropillar of 5 μm in diameter before and after FIB irradiation, respectively. (c) and (d), *idem* for micropillars of 2 μm in diameter and (e) and (f) *idem* for micropillars of 1 μm in diameter.

2.2. Compression tests

Micropillar compression tests were performed using a commercial Triboindenter TI 950 nanoindentation system from Hysitron, Inc. (Minneapolis, MN). Two flat punch diamond tips of 3 and 10 μm in diameter were used to apply the load, depending on the sample because the largest punch was too big to avoid contact with neighboring pillars in the samples with the smallest LiF fibers. The tests were performed under displacement control, with a feedback control loop of 78 kHz, and at a strain rate $(\Delta u/\Delta t)/L$ of approximately 10^{-3} s^{-1}.

Micropillars were considered cylindrical rods of length L_0 and cross-section A_0 to compute the stress and strain. For both as-grown and FIB machined micropillars, A_0 was taken as the top diameter of the pillar. In addition, it was assumed that volume of the micropillar was constant during deformation and the compressive stress and strain were given by:

$$\varepsilon = \ln\left(\frac{L_0 - u}{L_0}\right) \quad \text{and} \quad \sigma = \frac{P}{A_0}\left[1 - \frac{u}{L_0}\right] \tag{1}$$

where u is the applied displacement and P is the load.

It should be pointed out that the measured displacement is affected by the compliance of the surrounding matrix material at the base of the pillar. Therefore, the measured load–displacement curves have to be corrected for this extra compliance. Previous investigations in micropillars manufactured by FIB machining (Greer et al., 2005) used the Sneddon correction (Sneddon, 1965) to account for the sink-in effect at the base of the pillar, assuming that the pillar behaves as a perfectly rigid flat punch indenting the substrate. However, this approximation is not valid in this case because the micropillars are part of a continuous fiber that is embedded into another material, as shown schematically in Fig. 3(a). The correction for the compliance associated with the elastic deflection of the matrix at the base of the pillar can be obtained from the standard shear lag model for load transfer between the matrix and the fiber in an isolated fiber embedded in an infinite matrix (Cox, 1952). Assuming a perfect interface between pillar and matrix, the stress on the pillar σ is related to the shear stress at the interface τ according to:

$$\frac{d\sigma}{dx} + \frac{4\tau}{d} = 0, \quad x > L \tag{2}$$

where d stands for the pillar diameter. Eq. (2) can be solved assuming a simple linear relationship between the shear stress and the displacement at the interface u, $\tau = ku$ (Cox, 1952). The displacement of the top of the pillar u_0 subjected to a compressive stress σ_0 is then given by:

$$u_0 = \frac{\sigma_0}{E_{LiF}}\left(L_0 + \sqrt{\frac{E_{LiF}d}{4k}}\right), \tag{3}$$

where E_{LiF} stands for the elastic modulus of the pillar and k is expressed as

$$k = \frac{2G_{NaCl}}{d\log\left(\frac{2R_{eq}}{d}\right)} \tag{4}$$

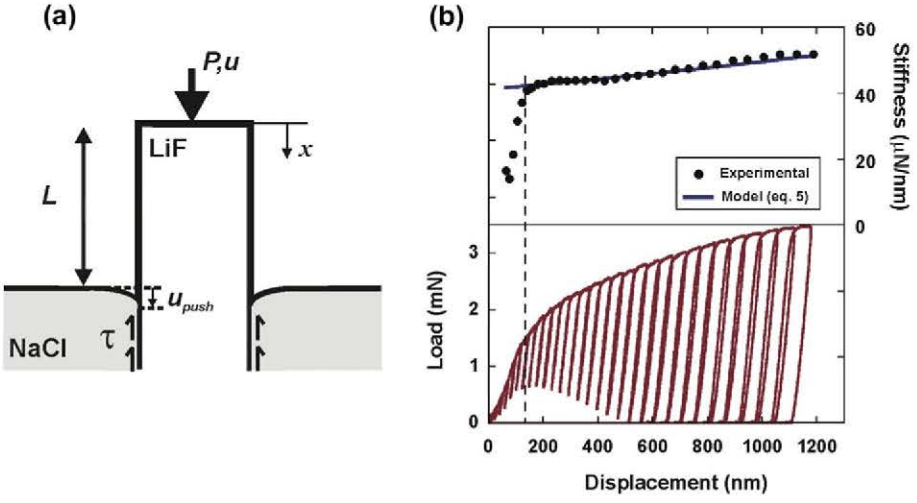

Fig. 3. (a) Schematic illustration of the compressed micropillar, showing the extra compliance due to the elastic deflection of the matrix at the base of the pillar. (b) Evolution of the stiffness of a micropillar of 2.5 μm in diameter as a function of the applied compressive displacement. The experimental stiffness was determined from the slope of the of the load–displacement segment during unloading and is compared with the theoretical value given by Eq. (5).

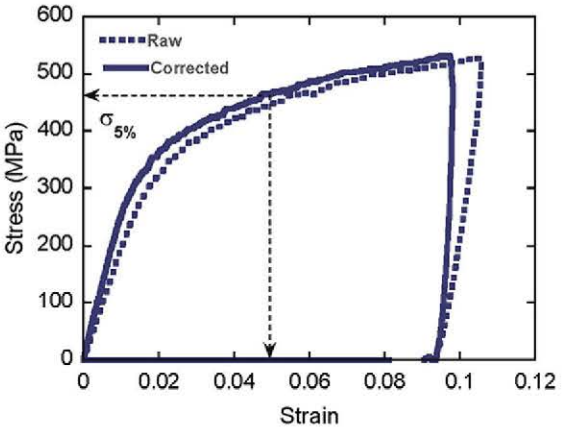

Fig. 4. True stress–strain curve of a micropillar of 5 μm in diameter computed with and without including the matrix compliance correction.

under the assumption that the vertical displacement of the matrix is 0 at a distance R_{eq} from the pillar center and where G_{NaCl} is the shear modulus of the matrix. Therefore, the total compliance of the pillar can be written according to Eq. (3) as:

$$C = \frac{4L}{\pi E_{LiF} d^2}\left[1 + \frac{d}{L}\sqrt{\frac{E_{LiF}\log(2R_{eq}/d)}{4G_{NaCl}}}\right] = \frac{4L}{\pi E_{LiF} d^2}\left[1 + \frac{d}{L}n\right] \tag{5}$$

where n is a constant that depends on the micropillar and matrix elastic moduli ratio and on a geometrical factor R_{eq}. The first term in Eq. (5) corresponds to the compliance of the pillar while the second term reflects the elastic deflection of the matrix at the base of the pillar.

In order to test the validity of this model, several pillars were subjected to multiple loading–unloading compression tests to measure the evolution of the pillar stiffness as a function of the applied displacement u. Fig. 3(b) shows one representative load–displacement curve together with the micropillar stiffness determined from the slope of each unloading segment. The linear increase in stiffness with the applied displacement was perfectly captured by Eq. (5), demonstrating the validity of the model. Note that the micropillar stiffness was lower than the theoretical one for very small displacements (<100 nm), and this discrepancy could be attributed to an extra compliance during the first stages of the test until full contact is established between the flat-punch and the top of the pillar.

It should also be noted that this stiffness correction had a marginal effect on the stress–strain curve, as shown in Fig. 4. In fact, these curves demonstrate that the matrix behavior did not significantly influence the micropillar compression tests. Nevertheless, the stiffness correction was important for a precise determination of the micropillar elastic modulus from the unloading segment of the load–displacement curve, leading to values very close to 146.5 GPa, the reported value for LiF in the [1 1 1] direction (Hard, 1968).

The initial elastic loading segment (Fig. 4) was more compliant than the final unloading, very likely due to the contact issues mentioned above and this fact made difficult to establish a yield stress from the stress–strain curve. To avoid this problem, the flow stress at 5% strain, $\sigma_{5\%}$, (Fig. 4) was used throughout this investigation as the characteristic value to compare the compressive strength of different pillars.

2.3. Crystal plasticity model

A crystal plasticity (CP) model was developed and implemented in the commercial finite element analysis program ABAQUS (Abaqus, 2008) to give insight into the dominant deformation mechanisms during uniaxial compression of the LiF micropillars. The CP model follows the classical work of Hill and Rice (Rice, 1971; Hill and Rice, 1972), assuming a multiplicative decomposition of the deformation gradient $\boldsymbol{F}$ into its elastic $\boldsymbol{F_e}$ and plastic part $\boldsymbol{F_p}$:

$$\boldsymbol{F} = \boldsymbol{F_e}\boldsymbol{F_p}. \tag{6}$$

The actual value of the velocity gradient $L = \dot{F}F^{-1}$ is obtained by taking the derivative of Eq. (6), leading to:

$$\boldsymbol{L} = \boldsymbol{L_e} + \boldsymbol{F_e}\boldsymbol{L_p}\boldsymbol{F_e}^{-1} \tag{7}$$

where the plastic velocity gradient, $\boldsymbol{L_p}$, is obtained by the sum of the shear rates, $\dot{\gamma}$, for each slip system, α, according to:

$$\boldsymbol{L_p} = \sum_{\alpha}\dot{\gamma}_{\alpha}(\boldsymbol{s}^{\alpha} \otimes \boldsymbol{m}^{\alpha}) \tag{8}$$

where $\boldsymbol{s}^{\alpha}$ and $\boldsymbol{m}^{\alpha}$ stand for the unit vectors in the slip direction and the normal to the slip plane, respectively, in the reference configuration. Two sets of slip systems, $\{1\,1\,0\}\langle 1\,1\,0\rangle$ and $\{1\,0\,0\}\langle 1\,1\,0\rangle$, which are known to be responsible for the plastic deformation in LiF were included in the crystal plasticity model (Dimiduk et al., 2010; Gilman, 1959).

The crystal is assumed to behave as an elasto-viscoplastic solid in which the plastic strain rate follows a power-law hardening expressed as (Hutchinson, 1976):

$$\dot{\gamma}_\alpha = \dot{\gamma}_o \left(\frac{\tau_\alpha}{\tau_y} \right)^{1/m} \tag{9}$$

where $\dot{\gamma}_o$ is a reference strain rate, τ_y the slip resistance, and m the rate sensitivity exponent. τ_α stands for to the resolved shear stress on the slip plane, which is obtained as the projection of the Kirchoff stress on the slip system:

$$\tau_\alpha = \mathbf{C} \left[\left(\boldsymbol{F}_e^{\mathrm{T}} \boldsymbol{F}_e \right)^{1/2} - \boldsymbol{I} \right] : \boldsymbol{s}^\alpha \otimes \boldsymbol{m}^\alpha \tag{10}$$

where $\boldsymbol{C}$ stands for the elastic stiffness tensor of the crystal.

The evolution of the critical shear stress τ_y^α for a given slip system, α, was obtained using the classical hardening model of Peirce et al. (1982), which defines the current slip resistance as:

$$\tau_y^\alpha = h_{\alpha\alpha}(\Gamma)\dot{\gamma}_\alpha + \sum_{\beta \neq \alpha} q_{\alpha\beta} h_{\alpha\alpha}(\Gamma)\dot{\gamma}_\beta \tag{11}$$

where q is the latent hardening constant, and $h_{\alpha\alpha}$ is referred to as the hardening modulus,

$$h_{\alpha\alpha}(\Gamma) = h_0 \operatorname{sech} \left| \frac{h_0 \Gamma}{\tau_s - \tau_0} \right|^2 \tag{12}$$

where h_0 is the initial hardening modulus, τ_0 the initial yield stress, τ_s the saturation yield stress, and Γ is the accumulated shear strain in all slip systems as given by,

$$\Gamma = \int_0^t \left(\sum_\alpha \dot{\gamma}_\alpha \right) dt \tag{13}$$

3. Experimental results

3.1. Compressive behavior of as-grown micropillars

As-grown micropillars tested in compression presented a large scatter in mechanical response, regardless of the micropillar diameter. Typical load–displacement curves are plotted in Fig. 5(a). After the initial elastic region, one set of micropillars presented a non-linear region with continuous hardening until a plateau was reached (marked 1 in Fig. 5(a)). Another set of micropillars presented, however, a marked softening shortly after yielding (marked 3 in Fig. 5(a)). Finally, micropillars with an intermediate behavior (marked 2 in Fig. 5(a)) were also found, in which the softening region started at higher loads, after the micropillar had underwent significant plastic strain hardening. The origin of the differences in mechanical response was evident when the compressed micropillars were observed in the SEM, as shown in Fig 5(b). Micropillars which presented continuous hardening until the maximum strength was attained remained straight upon deformation and two set of slip lines were visible (marked with black arrows) running from the top of the micropillar. On the contrary, micropillars which presented marked softening also showed significant bending in addition to compression upon deformation and the bending component increased with the amount of softening. The experimental procedure was carefully revised to ensure that this behavior reflected the actual response of the micropillars, which could be attributed to small misalignments in the crystal orientation resulting from instabilities during directional solidification (Llorca and Orera, 2006). It should be noted, however, that previous studies (Choi et al., 2007) did not report such a large influence of micropillar misalignment on the compressive response but these results were obtained in crystals whose plastic anisotropy was much lower than that of LiF. The hypothesis that the plastic anisotropy of LiF was responsible for the variability in the mechanical response will be analyzed in detail in Section 4 with the aid of crystal plasticity simulations.

These results show the significant influence that initial tilt/misalignments, difficult to control due to small variations from grain to grain along the eutectic microstructure, have in the compression behavior of LiF [1 1 1] oriented micropillars. To eliminate this variable, only those micropillars that did not show any significant bending during deformation were used for the remaining of this investigation to avoid the scatter associated with the random initial misalignment. This led to a very good reproducibility in the mechanical response for all micropillar diameters with a noticeable increase of the scatter for the 1 μm pillar diameter. Fig. 6(a)–(c) plot compressive stress–strain curves of as-grown micropillars of 5, 2.5 and 1 μm in diameter, respectively, while the evolution of the flow stress at 5% strain, $\sigma_{5\%}$, with micropillar diameter is plotted in Fig. 6(d). The plots do not show any noticeable size effect on the mechanical response of LiF [1 1 1] as-grown micropillars in the range of pillar diameters studied. The flow stress at 5% strain was around 500 MPa in all cases.

The larger scatter, together with the more jerky behavior, of the stress–strain curves of the 1 μm pillars is consistent with the experimental evidence in metallic micropillars as the available dislocation sources are progressively exhausted (Ng and

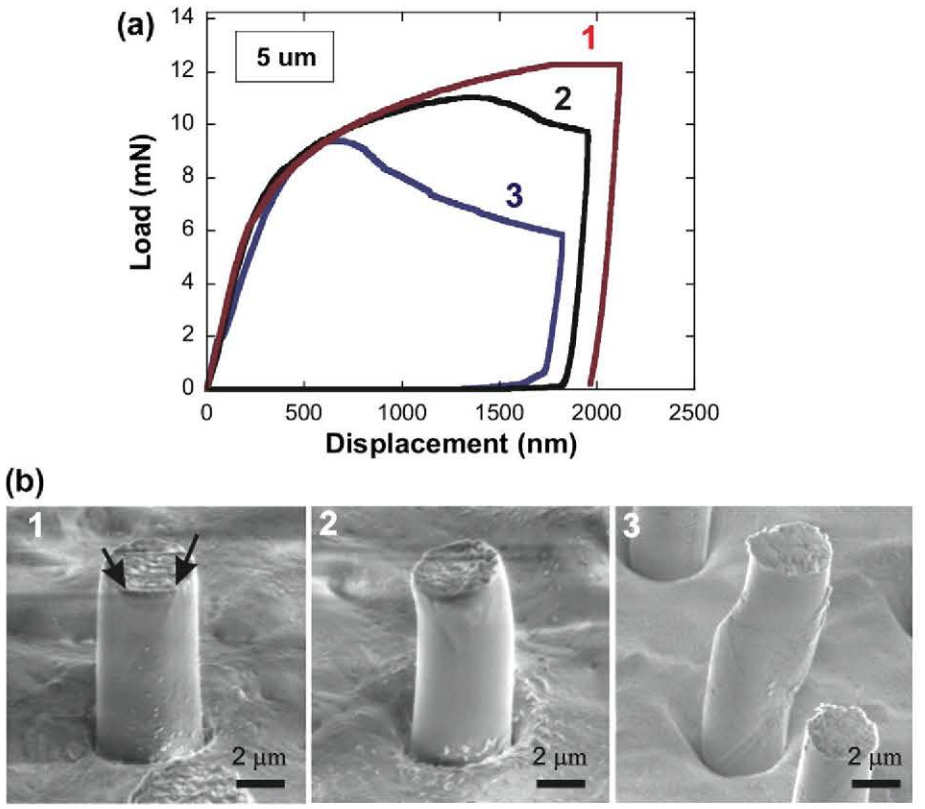

Fig. 5. (a) Selected load–displacement curves showing the variability in the mechanical response of LiF micropillars oriented in the [1 1 1] direction. (b) SEM images of the compressed micropillars, corresponding to the load–displacement curves in (a), showing that bending of the pillar results in a reduced compressive load (see curves 2 and 3). Note the slip bands that can be seen in the surface of pillar 1, as a result of the compressive deformation.

Ngan, 2008a,b,c; Ngan and Ng, 2010). The number of available dislocation sources decreases with the micropillar diameter, and a transition is found in the stress–strain curves for a critical micropillar size. Micropillars larger than the critical size present smooth stress–strain curves and limited scatter while the stress–strain curves of micropillars below the critical size present strain instabilities and more scatter. The former correspond to micropillars of 5 and 2 μm in diameter in Fig. 6a and b, while the latter stands for the response of micropillars of 1 μm in diameter in Fig. 6c. It should be noticed, however, that size effects were not observed in the range of pillar diameters studied (1–5 μm) in LiF micropillars compressed along the [1 1 1] direction.

In order to understand the results of these tests, it is important to analyze the plastic deformation micromechanisms in LiF single crystals. As mentioned in the introduction, two different slip systems can be activated in LiF depending on crystal orientation: the "soft" $\{1\,1\,0\}\langle 1\,1\,0\rangle$ and the "hard" $\{1\,0\,0\}\langle 1\,1\,0\rangle$ slip systems. Johnston and Gilman (Johnston and Gilman, 1959; Gilman, 1959), who extensively studied the plastic deformation of LiF single crystals, reported a critical resolved shear stress on the "soft" slip system $\{1\,1\,0\}\langle 1\,1\,0\rangle$ at 10^{-3} s^{-1} strain rate and room temperature of the order of 8–15 MPa, depending on initial dislocation density. In the case of the "hard" slip system $\{1\,0\,0\}\langle 1\,1\,0\rangle$, there are no data at room temperature for bulk crystals because of their brittle behavior. Extrapolation of high temperature results to room temperature points to ratios of the critical resolved shear stresses between the hard and the soft slip systems, τ_{hard}/τ_{soft}, of the order of 10–20 (Gilman, 1959), which denotes a very high plastic anisotropy. In our case, the LiF micropillars were oriented in the [1 1 1] direction and the Schmid factor corresponding to all "soft" slip systems was zero. Thus, only three "hard" slip systems of the family $\{1\,0\,0\}\langle 1\,1\,0\rangle$, with a Schmid factor of 0.47, could be initially activated. This is compatible with the slip traces observed in the surface of the micropillars which remained straight during deformation (Fig. 5(b)).

The fact that micropillar compression of LiF [1 1 1] yields plastic deformation and not fracture is an indication that the small size suppressed cracking, as shown elsewhere (Östlund et al., 2011), and highlights the benefit of using micropillar compression to study plasticity in brittle materials without the need of using complex tests, like compression under confining pressure. The measured flow stress of ≈500 MPa leads to an estimation of the critical resolved shear stresses for the hard slip system of the order of 250 MPa, which is reasonable for bulk LiF (Gilman, 1959), although the exact value is very sensitive to impurities and dislocation density. This result is in agreement with the lack of a size effect on the flow stress of as-grown LiF [1 1 1] micropillars observed in this work.

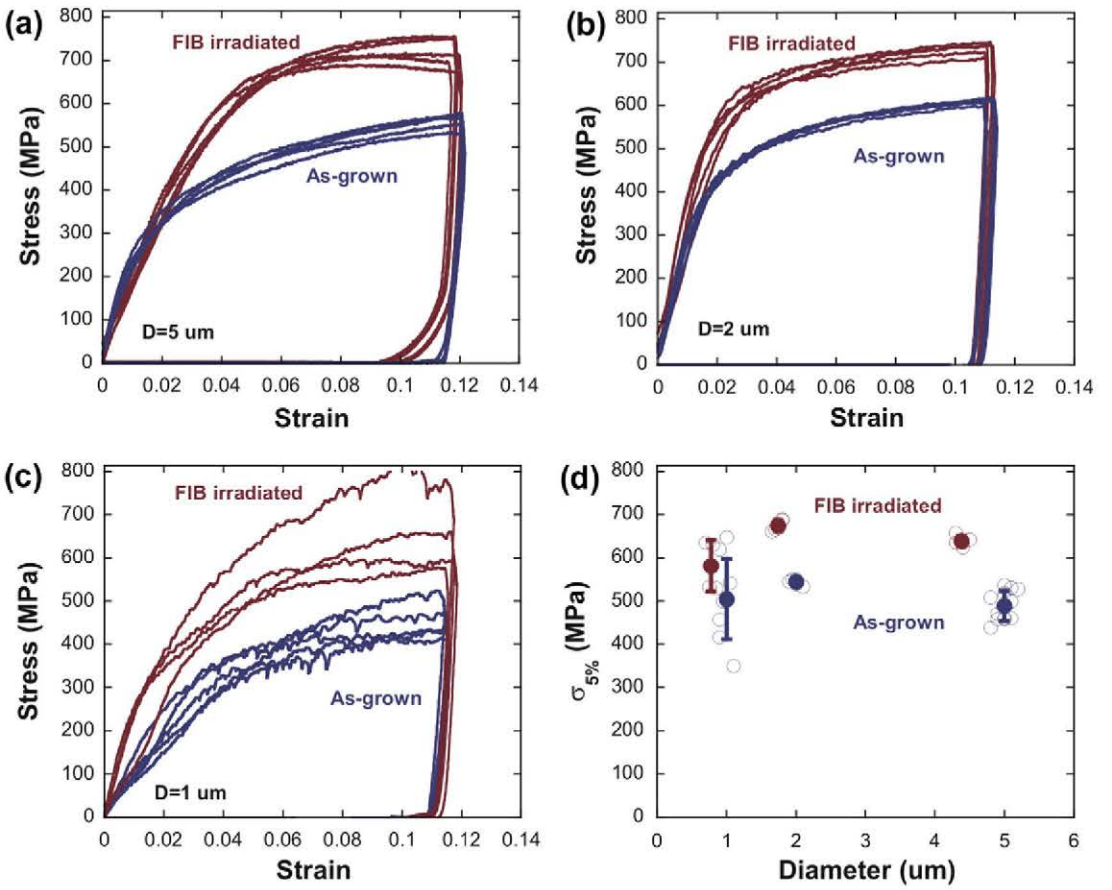

Fig. 6. Compressive stress–strain curves of micropillars of (a) 5 μm, (b) 2.5 μm and (c) 1 μm in diameter, respectively, before and after ion irradiation. (d) Flow stress at 5% strain, $\sigma_{5\%}$, as a function of diameter for as-grown and ion irradiated micropillars.

3.2. Effect of ion irradiation

Representative stress–strain curves of the micropillars which were subjected to ion irradiation are plotted in Fig. 6(a)–(c) for different micropillar diameters, together with the curves corresponding to the as-grown micropillars. The stress–strain curves of the irradiated micropillars of 5 and 2 μm in diameter were very reproducible while those of the 1 μm micropillars presented slightly more scatter, as in the case of the as-grown pillars. The flow stress at 5% strain, $\sigma_{5\%}$, of as-grown and ion irradiated micropillars is plotted in Fig. 6(d), as a function of the micropillar diameter. It shows that ion irradiation increased the flow stress by 30% in all cases. This result is in agreement with previous observations in bulk LiF which have established that the bulk yield stress of LiF is very sensitive to ion irradiation (Johnston and Gilman, 1959). The exact origin of this irradiation hardening is unknown but the current understanding indicates that the increased resistance to dislocation motion in irradiated LiF is mainly due to randomly distributed halogen interstitials (the so-called H- and V-centers) forming clusters of different sizes. In any case no size effects on the flow stress were observed in either the as-grown or the ion irradiated micropillars.

4. Effect of micropillar misalignment

Three-dimensional finite element simulations of the compression tests were carried out to check the hypothesis that the large variability in the stress–strain curves could be due to the slight initial misalignment of the pillar with respect to the [1 1 1] direction. The perfectly aligned micropillar (0° tilt angle) was modeled as a cylinder of 5 μm in diameter and 10 μm in length, according to the aspect ratio of actual micropillars. The [1 1 1] lattice orientation was parallel to the loading axis. Small misalignments of the crystal with respect to the loading axis were simulated by shearing the cylinder by an angle equal to the tilt, while the top and bottom surfaces of the cylinder were kept parallel to the base and the surface of the flat indenter, as shown in Fig. 7. The [1 1 1] lattice orientation was consequently parallel to the cylinder axis.

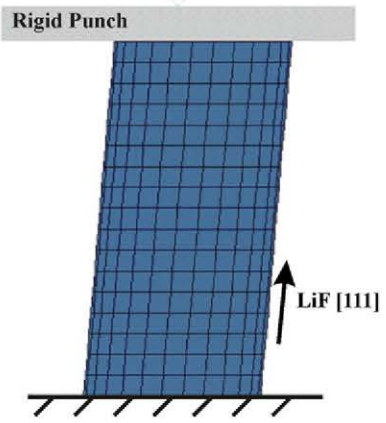

Fig. 7. Finite element model of a [1 1 1] LiF micropillar tilted 5° with respect to the loading axis, showing the mesh and the boundary conditions. The indenter tip was modeled as a rigid surface, with a lateral stiffness of 10 μN/nm, and a Coulombian friction model was used to model the micropillar-tip contact was with a friction coefficient of 0.1. The [1 1 1] orientation is parallel to the cylinder axis.

Table 1
Elastic constants of LiF single crystal (Hard, 1968) and parameters that define the evolution of the critical resolved shear stress in each slip system according to Eqs. (11) and (12).

Elastic constants			
c_{11} (GPa)	c_{12} (GPa)	c_{44} (GPa)	
114.2	47.9	63.6	
Crystal plasticity parameters			
Slip system	τ_0 (MPa)	τ_S (MPa)	h_0 (MPa)
{1 0 0}⟨1 1 0⟩	210	360	1400
{1 1 0}⟨1 1 0⟩	10.5	18	70

Boundary conditions were designed to mimic the experiments. The base of the pillar was fully constrained. The flat tip was modeled as a rigid solid, with a lateral stiffness of 10 μN/nm (comparable to the lateral stiffness of the indenter used in the experiments). A Coulombian friction model was used to model the micropillar-tip contact, with a friction coefficient of 0.1. The cylinder was discretized with approximately 1500 8-node quadratic elements (C3D8 in Abaqus). A typical finite element model of micropillar tilted by 5° is shown in Fig. 7. The crystal behavior followed the crystal plasticity model presented above. The elastic constants of the cubic LiF crystal were taken from literature and can be found in Table 1. The plastic deformation of each slip system was controlled by the parameters τ_0^α, τ_S^α and h_0^α. Those for the "hard" slip system {1 0 0}⟨1 1 0⟩ were obtained by fitting the simulated stress–strain curve with the experimental curves of the 5 μm micropillars that remained straight upon deformation. In order to reduce the number of adjustable parameters, the latent hardening coefficients, $q_{\alpha\alpha}$, were set to 1. The values obtained after the fitting were in good agreement with the expected bulk experimental value (Gilman, 1959), with $\tau_0 = 210$ MPa for the hard slip system, very close to the 250 MPa estimated in this work. The same constitutive law was assumed for the soft slip systems, but the critical resolved shear stress was reduced by a factor of 20, according to the literature (Johnston and Gilman, 1959). The parameters that define the evolution of the critical resolved shear stress in each slip system according to Eqs. (11) and (12) are summarized in Table 1. The reference strain rate and the rate sensitivity were given by $\dot{\gamma}_0 = 1\ s^{-1}$ and $m = 0.1$. Simulations of compression of LiF [1 1 1] micropillars with initial tilts of 0°, 2°, and 5° were carried out with Abaqus/Standard within the framework of the finite deformations theory with the initial unstressed state as reference.

The effect of the initial misalignment (0°, 2° and 5°) on the compressive stress–strain curve is plotted in Fig. 8(a), together with the experimental curves (dashed lines) taken from Fig. 5(a). The numerical simulations demonstrate that a small misalignment in the micropillar orientation leads to a dramatic effect in the shape of the stress–strain curve, which reproduces very accurately the experimental results reported above. This large effect of the initial tilt contrasts with previous simulations (Choi et al., 2007; Raabe et al., 2007) that predicted a very small effect of the initial misorientation on the flow stress. However, these analyses were carried out in fcc single crystals with very limited plastic anisotropy as opposed to LiF which presents a large difference in the critical resolved shear stress between the soft and the hard slip systems. Indeed, the effect of the initial tilt angle of the stress–strain curve is almost negligible if the plastic anisotropy is removed by making $\tau_{hard} = \tau_{soft}$, as shown in Fig. 8(b).

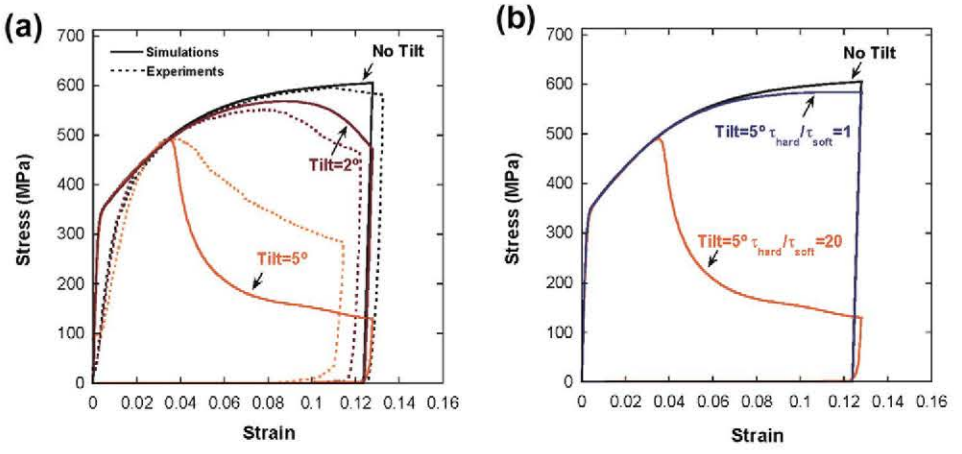

Fig. 8. (a) Simulated (solid lines) and experimental (dashed lines) compressive stress–strain curves of LiF micropillars. The simulated curves correspond to micropillars with an initial misalignment of 0°, 2° and 5°. (b) Simulated compressive stress–strain curves in the absence of plastic anisotropy for micropillars with an initial misalignment 0° and 5°. Tilt has a negligible effect on the mechanical response in this case.

The mechanisms of deformation responsible for the mechanical response are readily understood from the contour plots of the accumulated plastic strain, of Fig. 9, in two particular slip systems: one soft, the (101)[10−1], and one hard, the (001)[110], for an applied compressive engineering strain of 12%. Only the hard slip systems were activated in the micropillar with 0° tilt, which remained straight upon loading, while the soft slip systems were inactive as their Schmid factor was 0 (Fig. 9(a)). As a result, the micropillar presented continuous strain hardening and the flow stress was controlled by the hard slip system. However, a slight initial misalignment led to the activation of the soft slip system and to the rotation of the micropillar, increasing the Schmid factor of the soft slip systems. As a result, plastic strain was localized in the soft slip system in the micropillar with an initial tilt of 5° while the hard slip systems absorbed very little plastic deformation (Fig. 9c). Once deformation was controlled by the soft slip system, the flow stress of the micropillar decreased rapidly, leading to the softening regime experimentally observed. The micropillar with 2° misorientation (Fig. 9(b)) presented an intermediate behavior between the previous ones. Finally, if the plastic anisotropy of the crystal is removed by making $\tau_{hard}/\tau_{soft} = 1$, small misalignments are not able to activate the soft slip system because the Schmidt factor is too low compared with the hard slip system (Fig. 9(d)). As a result, the soft slip system is not activated and the micropillar does not bend upon compression. These results show that materials which present a marked plastic anisotropy are be much more sensitive to initial tilts/misalignments of the pillars with respect to the compression axis than plastically isotropic solids like fcc and bcc metals.

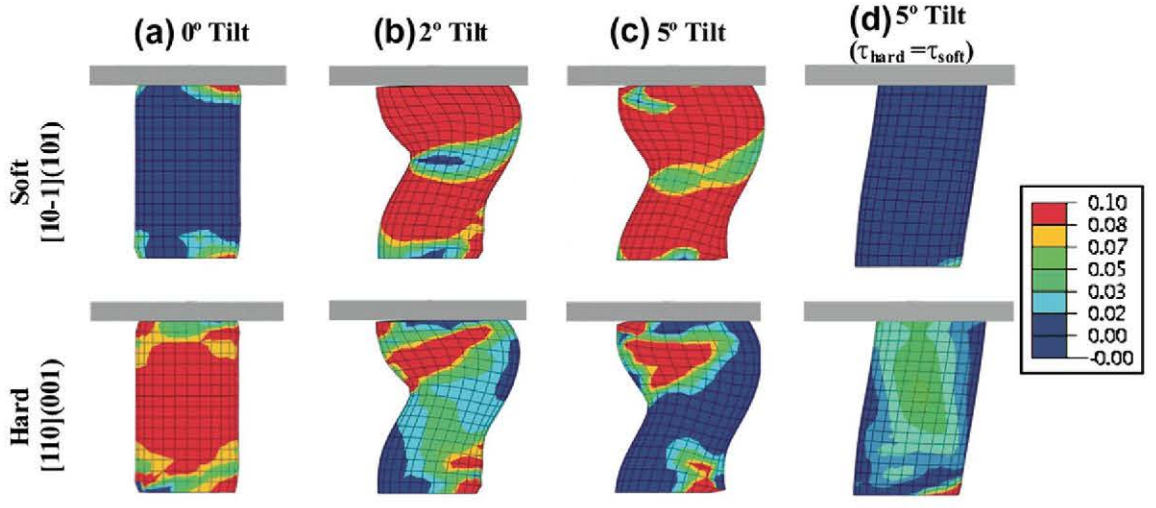

Fig. 9. Contour plots of accumulated plastic strain in the soft (above) and the hard (below) slip systems for different initial tilts angles: (a) 0° (b) 2° (c) 5° (d) 5° for a material in which $\tau_{hard}/\tau_{soft} = 1$. The applied compressive engineering strain was 12% in all cases.

5. Effect of micropillar size and ion irradiation

Our results contrast with previous studies that have shown strong size effects in the plastic deformation of fcc metals (Uchic et al., 2004; Greer et al., 2005; Volkert and Lilleodden, 2006) and ionic compounds (Nadgorny et al., 2008; Dimiduk et al., 2010). In particular, Nadgorny et al. (2008) reported a strong size effect in [1 0 0] oriented LiF micropillars fabricated by FIB when the micropillar diameter was in the range 1–10 μm. The discrepancies between these results and those reported in this paper can be attributed to three causes: differences in the initial dislocation density, FIB machining and crystal orientation.

The LiF [1 0 0] micropillars of Nadgorny et al. (2008) were machined from bulk crystals with a very low initial dislocation density (10^9 m^{-2}) but it should be noted that the real dislocation density on the FIB machined micropillars was likely to be much higher than that of the bulk crystals because of the effect of ion irradiation. Otherwise, the micropillars would have been virtually dislocation-free, displaying a whisker-type behavior, which was not the case. It was not possible to determine the initial dislocation density in our LiF [1 1 1] pillars because they are not produced from bulk crystals, but by directional solidification of an eutectic mixture. However, the fact that these micropillars did not display a whisker-type behavior, controlled by the nucleation of dislocations (as the one observed in the Mo micropillars of Bei et al. (2008)), indicates the existence of an initial dislocation network caused by the thermal residual stresses developed upon cooling because of the differences in the coefficients of thermal expansion of both phases in the eutectic. So, both LiF micropillars in Nadgorny et al. (2008) and in this investigation contained a network of mobile dislocations prior to testing although the actual densities are unknown.

Another origin of the differences may be FIB milling. Previous studies in metals have reported that FIB machining leads to Ga^+ ion implantation and to the formation of dislocation networks within a damaged surface layer of several nanometers in depth (Kiener et al., 2007), but that these surface defects are driven out by mechanical annealing upon loading, at least in sub-micron pillars (Shan et al., 2007). As a result, the extended view points to the conclusion that the effect of FIB milling on metallic micropillar compression is negligible provided the pillar has some initial dislocation structure before milling (El-Awady et al., 2009), that provides an initial distribution of dislocation sources. This way the truncation of dislocation sources originates the size effects (Parthasarathy et al., 2007; Rao et al., 2008; Akarapu et al., 2010; Ngan, 2011). Recent studies in mechanically pre-strained Mo pillars, both with (Schneider et al., 2010) and without FIB milling (Shim et al., 2009), support this view, because size effects are independent of whether the initial defect distribution is due to FIB machining or mechanical pre-strain. This seems also to be the case for the [1 0 0] oriented LiF micropillars, but not the for [1 1 1] oriented LiF pillars reported in this work.

On the contrary, this paper shows that the flow stress of [1 1 1] oriented LiF pillars, both in the as-grown and FIB machined condition, is independent of pillar size and that FIB machining increases the flow stress by 30%, for all pillar diameters. Even though the type of defects that FIB machining introduces in ionic compounds has not been documented up to date, our results point to the conclusion that the mechanical behavior of the [1 1 1] oriented micropillars is not controlled by the distribution of dislocation sources. The origin of this discrepancy has to be found in the high Peierls stress of active slip systems in the [1 1 1] oriented LiF micropillars. In the case of [1 0 0] oriented LiF micropillars, compression takes place by the activation of the soft slip systems, while LiF micropillars perfectly oriented along the [1 1 1] deform in compression by plastic deformation along the hard slip systems. The critical resolved shear stress obtained by us in [1 1 1] LiF and by Nadgorny et al. (2008) in [1 0 0] LiF are plotted in Fig. 10 as a function of micropillar diameter. Representative values for the bulk critical resolved shear stresses for the soft and hard slip systems are indicated as reference (Johnston and Gilman, 1959; Gilman, 1959). The direct comparison of these values with those obtained from micropillar compression should be done with care since they depend on impurity level, dislocation density and strain rate, and the former two are not known in the micropillar compression tests. That is why the bulk values are indicated as a range in Fig. 10.

The data in Fig. 10 suggest that the size effect depends on the magnitude of the bulk shear yield stress, so that the higher the bulk shear yield stress the lower the size effect. This hypothesis was first advanced by Korte and Clegg, 2010, as they found a similar behavior in [1 0 0] and [1 1 1] MgO micropillars, a material with the same crystal structure than LiF. The empirical law typically used to represent size effects has the form:

$$\tau_{CRSS} = \tau_0 + Kd^{-n} \tag{14}$$

where τ_0 represents the bulk shear yield stress and the second term includes the hardening contributions associated with size. The main contributions to τ_0 in pure single crystals are the lattice resistance due to the Peierls stress and the forest dislocation hardening. When τ_0 is very small, as in fcc metals and LiF [1 0 0], size effects, due for instance to the truncation of dislocation sources, control the mechanical response of the micropillars, which present size exponents in the range $n \sim 0.6$ to ~ 0.8. In the case of bcc metals, with a higher Peierls potential, the influence of the size effect on the crystal hardening is less marked and lower size effects have been reported, with n in the range 0.21–0.48 (Schneider et al., 2009a,b; Greer et al., 2008). This is supported by recent data on various bcc metals suggesting that n was directly linked to the screw dislocation mobility (hence the Peierls potential) at the test temperature (Schneider et al., 2009a,b). Finally, strong solids with very high Peierls stress, like GaAs (Michler et al., 2007), Si (Moser et al., 2007) and LiF {1 0 0}⟨1 1 0⟩ (this work), show virtually no size effect on the flow stress, with $n \sim 0.1$. It appears therefore that the compressive flow stress of micropillars in materials with high lattice resistance is governed by the bulk yield stress, while size effects associated with the operation of dislocation

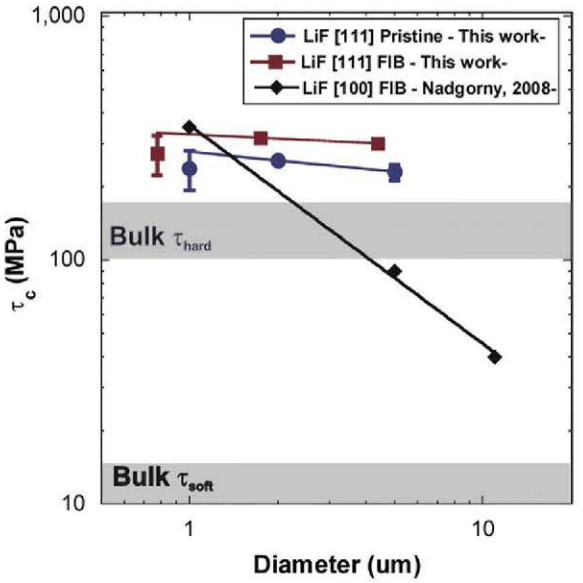

Fig. 10. Critical resolved shear stress in LiF [1 1 1] obtained in this work and in LiF [1 0 0] (Nadgorny et al., 2008) as a function of micropillar diameter.

sources, if any, are of smaller magnitude than the bulk yield stress, and thus irrelevant. One benefit of the lack of size effects is the ability to use micro and nanomechanical testing to study the bulk plastic deformation of brittle strong solids without the need of using complex tests, like compression under confining pressure, to avoid cracking.

In view of this, the differences in flow stress between the as-grown and ion-irradiated [1 1 1] LiF pillars (around 30%) can be attributed to the increase in bulk yield stress due to ion irradiation. Although the exact nature and extent of the FIB-induced defects in LiF is unknown, a plausible explanation is the generation of randomly distributed halogen interstitials that increase the lattice resistance, and that this damage extends deeper in the material than encountered for metallic pillars, contributing to an increase of the bulk yield stress, independently of the diameter of the pillar.

Finally, this work shows that micropillar compression of highly anisotropic crystals is very sensitive to the crystal orientation. Very small misalignments can induce large variations in the stress–strain curve, including softening as shown in Fig. 8, because slip systems with very low Schmid factors might begin to dominate the compression behavior due to the large discrepancies in critical resolved shear stresses between the "soft" and the "hard" orientations. This contrasts with previous studies based on crystal plasticity simulations of fcc metals pointing out that misalignment has strong effects on the apparent elastic modulus but that the flow stress is only affected by a few percent (Choi et al., 2007). Other experimental parameters can also have strong effects on the stress–strain curve, such as the lateral constrain imposed by the indenter. According to experimental evidence and crystal plasticity simulations in fcc metals (Raabe et al., 2007; Shade et al., 2009), high lateral constrain results in lower yield stress and higher strain hardening because the large rotations in the constrained situation result in the activation of secondary slip systems. In addition, a breakdown of Schmid law in the case of sub-micron diameter pillars has been reported in crystals with a single family of slip systems due to the limited number of available dislocation sources when the diameter is reduced (Ng and Ngan, 2008a,b,c), which could result in stochastic activation of sources in non-preferred slip systems. Further work is needed to study these effects in plastically anisotropic crystals and LiF constitutes an idea model material to do so.

6. Conclusions

Compression tests were carried out in LiF single crystals micropillars oriented in the [1 1 1] direction obtained by etching the matrix in directionally-solidified eutectic crystals. Micropillars with diameters in the range 1–5 μm, in the as-grown condition or after ion irradiation by FIB were tested. Ion irradiation led to an increase of approximately 30% on yield strength and the maximum compressive strength. It was also found that small misalignments (below 5°) in the initial orientation of the LiF micropillars led to large differences in the flow stress and the active slip systems. Crystal plasticity simulations of the compressive deformation showed that this behavior was characteristic of crystals which present a large difference in the flow stress between different slip systems.

No effect of the micropillar diameter on flow stress was found in either the as-grown or the ion irradiated pillars, in contrast to previous studies in LiF micropillars oriented in the [1 0 0] direction and manufactured by FIB which showed a strong size effect on the flow stress (Nadgorny et al., 2008). The discrepancy between both investigations was explained based on the different behavior of the soft and hard slip systems of LiF, with the soft slip system showing a strong size effect on the

flow stress – similar to those found in fcc metals – while the hard slip system did not show any significant size effect. These results are in agreement with previous studies (Korte and Clegg, 2010) pointing out that the extent of the size effect on the flow stress scales with the bulk lattice resistance of the material: i.e., materials with a significant lattice resistance – like bcc metals, Si, GaAs and LiF deformed along the hard slip system – show much less pronounced size effects than materials where the lattice resistance is very small – like fcc metals and LiF deformed along the soft slip system.

Acknowledgements

R.S., J.M.M.A., J.S. and J.L. acknowledge the financial support of the Spanish Ministry of Science and Innovation (MAT2009-14396) and the Comunidad de Madrid through the program ESTRUMAT (S2009/MAT-1585) and the program PLASMOD (CCGIO-UPM/MAT-5404). V.M.O. and R.I.M. acknowledge the financial support of the CE with Grant Number ENSEMBLE-NMP4-SL-2008-213669. The authors are indebted to Maria Fernanda Acosta (ICMA) for her help in preparing some of the samples used in this study.

References

Abaqus, 2008. Users' Manual, version 6.7. ABAQUS, Inc.
Akarapu, S., Zbib, H.M., Bahr, D.F., 2010. Analysis of heterogeneous deformation and dislocation dynamics in single crystal micropillars under compression. Int. J. Plast. 26, 239–257.
Bei, H., Shim, S., George, E.P., Miller, M.K., Herbet, E.G., Pharr, G.M., 2007. Compressive strengths of molybdenum alloy micro-pillars prepared using a new technique. Scr. Mater. 57, 397–400.
Bei, H., Shim, S., Pharr, G.M., George, E.P., 2008. Effects of pre-strain on the compressive stress–strain response of Mo-alloy single-crystal micropillars. Acta Mater. 56, 4762–4770.
Brenner, S.S., 1958. Growth and properties of "whiskers". Science 128, 569–575.
Choi, Y.S., Uchic, M.D., Parthasarathy, T.A., Dimiduk, D.M., 2007. Numerical study on microcompression tests of anisotropic single crystals. Scr. Mater. 57, 849–852.
Cox, H.L., 1952. The elasticity and strength of paper and other fibrous materials. Brit. J. Appl. Phys. 3, 72–79.
Dehm, G., 2009. Miniaturized single-crystalline fcc metals deformed in tension: New insights in size-dependent plasticity. Prog. Mater. Sci. 54, 664–688.
Dimiduk, D.M., Nadgorny, E.M., Woodward, C., Uchic, M.D., Shade, P.A., 2010. An experimental investigation of intermittent flow and strain burst scaling behavior in LiF crystals during microcompression testing. Philos. Mag. 90, 3621–3649.
El-Awady, J.A., Woodward, C., Dimiduk, D.M., Ghoniem, N.M., 2009. Effects of focused ion beam induced damage on the plasticity of micropillars. Phys. Rev. B 80, 104104.
Gilman, J.J., 1959. Plastic anisotropy of LiF and other rock salt type crystals. Acta Metall. 7, 608.
Greer, J.R., De Hosson, J.T.M., 2011. Plasticity in small-sized metallic systems: intrinsic versus extrinsic size effect. Prog. Mater. Sci. 56, 654–724.
Greer, J.R., Nix, W.D., 2006. Nanoscale gold pillars strengthened through dislocation starvation. Phys. Rev. B: Condens. Matter 73, 245410.
Greer, J.R., Oliver, W.C., Nix, W.D., 2005. Size dependence of mechanical properties of gold at the micron scale in the absence of strain gradients. Acta Mater. 53, 1821–1830.
Greer, J.R., Weinberger, C.R., Cai, W., 2008. Comparing the strength of f.c.c. and b.c.c. sub-micrometer pillars: compression experiments and dislocation dynamics simulations. Mater. Sci. Eng. A 493, 21–25.
Hard, S., 1968. The measurement of the elastic constants of four alkali halides. J. Phys. D: Appl. Phys. 1, 1277.
Hill, R., Rice, J.R., 1972. Constitutive analysis of elastic–plastic crystals at arbitrary strain. J. Mech. Phys. Solids 20, 401.
Hutchinson, J.W., 1976. Bounds and self-consistent estimates for creep of polycrystalline materials. Proc. Roy. Soc. Lond. A 348, 1001–1127.
Jang, D., Gross, C.T., Greer, J.R., 2011. Effects of size on the strength and deformation mechanism in Zr-based metallic glasses. Int. J. Plast. 27, 858–867.
Johnston, W.G., Gilman, J.J., 1959. Dislocation velocities, dislocation densities and plastic flow in lithium fluoride crystals. J. Appl. Phys. 30, 129.
Kiener, D., Motz, C., Schöberl, T., Jenko, M., Dehm, G., 2006. Determination of mechanical properties of copper at the micron scale. Adv. Eng. Mater. 8, 1119–1125.
Kiener, D., Motz, C., Rester, M., Jenko, M., Dehm, G., 2007. FIB damage of Cu and possible consequences for miniaturized mechanical tests. Mater. Sci. Eng. A 459, 262–272.
Korte, S., Clegg, W.J., 2010. Discussion of the dependence of the effect of size on the yield stress in hard materials studied by microcompression of MgO. Philos. Mag. 91, 1150–1162.
Korte, S., Barnard, J.S., Stearn, R.J., Clegg, W.J., 2011. Deformation of silicon – insights from microcompression testing at 25–500 °C. Int. J. Plast. 27, 1853–1866.
Llorca, J., Orera, V.M., 2006. Directionally solidified eutectic ceramic oxides. Prog. Mater. Sci. 51, 711–809.
Maas, R., Van Petergem, S., Zimmermann, J., Borca, C., Van Swygenhoven, H., 2008. Scr. Mater. 59, 471–474.
Michler, J., Wasmer, K., Meier, S., Ostlund, F., Leifer, K., 2007. Plastic deformation of gallium arsenide micropillars under uniaxial compression at room temperature. Appl. Phys. Lett. 90, 043123.
Moser, B., Wasmer, K., Barbieri, L., Michler, J., 2007. Strength and fracture of Si micropillars: a new scanning electron microscopy-based micro-compression test. J. Mater. Res. 22, 1004–1011.
Nadgorny, E.M., Dimiduk, D.M., Uchic, M.D., 2008. Size effects in LiF micron-scale single crystals of low dislocation density. J. Mater. Res. 23, 2829–2835.
Ng, K.S., Ngan, A.H.W., 2008. Breakdown of Schmid's law in micropillars. Scr. Mater. 59, 796–799.
Ng, K.S., Ngan, A.H.W., 2008b. Stochastic theory for jerky deformation in small crystal volumes with preexisting dislocations. Philos. Mag. 88, 677–688.
Ng, K.S., Ngan, A.H.W., 2008c. Stochastic nature of plasticity of aluminum micro-pillars. Acta Mater. 56, 1712.
Ngan, A.H.W., Ng, K.S., 2010. Transition from deterministic to stochastic deformation. Philos. Mag. 90, 1937–1954.
Ngan, A.H.W., 2011. An explanation for the power-law scaling of size effect on strength in micro-specimens. Scripta Mater. 65, 978–981.
Orera, V.M., Larrea, A., 2005. NaCl-assisted growth of micrometer-wide long single crystalline fluoride fibres. Opt. Mater. 27, 1726.
Orera, V.M., Larrea, A., Merino, R.I., Rebolledo, M.A., Vallés, J.A., Gotor, R., Peña, J.I., 2005. Novel photonic materials made from ionic eutectic compounds. Acta Phys. Slova. 55, 261.
Östlund, F., Ghisleni, R., Howie, P.R., Korte, S., Leifer, K., Clegg, W.J., Michler, J., 2011. Ductile–brittle transition in micropillar compression of GaAs at room temperature. Philos. Mag. 91, 1190–1199.
Parthasarathy, T.A., Rao, S.I., Dimiduk, D.M., Uchic, M.D., Trinkle, D.R., 2007. Contribution to size effect of yield strength from the stochastics of dislocation source lengths in finite samples. Scr. Mater. 56, 313–316.
Peirce, D., Asaro, R.J., Needleman, A., 1982. An analysis of nonuniform and localized deformation in ductile single-crystals. Acta Metall. Mater. 30, 1087–1119.
Raabe, D., Ma, D., Roters, F., 2007. Effects of initial orientation, sample geometry and friction on anisotropy and crystallographic orientation changes in single crystal microcompression deformation: a crystal plasticity finite element study. Acta Mater. 55, 4567–4583.

Rao, S.I., Dimiduk, D.M., Parthasarathy, T.A., Uchic, M.D., Tang, M., Woodward, C., 2008. A thermal mechanisms of size-dependent crystal flow gleaned from three-dimensional discrete dislocation simulations. Acta Mater. 56, 3245–3259.
Rice, J.R., 1971. Inelastic constitutive relations for solids – an internal-variable theory and its application to metal plasticity. J. Mech. Phys. Solids 19, 433–455.
Schneider, A.S., Clark, B.G., Frick, C.P., Gruber, P.A., Arzt, E., 2009a. Effect of orientation and loading rate on compression behavior of small-scale Mo pillars. Mater. Sci. Eng. A 508, 241.
Schneider, A.S., Kaufmann, D., Clark, B.G., Frick, C.P., Gruber, P.A., Monig, R., Kraft, O., Arzt, E., 2009b. Correlation between critical temperature and strength of small-scale bcc pillars. Phys. Rev. Lett. 103, 105501.
Schneider, A.S., Clark, B.G., Frick, C.P., Gruber, P.A., Arzt, E., 2010. Effect of pre-straining on the size effect in molybdenum pillars. Phil. Ma. 90, 841–849.
Shade, P.A., Wheeler, R., Choi, Y.S., Uchic, M.D., Dimiduk, D.M., Fraser, H.L., 2009. A combined experimental and simulation study to examine lateral constraint effects on microcompression of single-slip oriented single crystals. Acta Mater. 57, 4580–4587.
Shan, Z.W., Mishra, R.K., Syed Asif, S.A., Warren, O.L., Minor, A.M., 2007. Mechanical annealing and source-limited deformation in submicrometre-diameter Ni crystals. Nat. Mater. 7, 115–119.
Shim, S., Bei, H., Miller, M.K., Pharr, G.M., George, E.P., 2009. Effects of focused ion beam milling on the compressive behaviour of directionally solidified micropillars and the nanoindentation response of an electropolished surface. Acta Mater. 57, 503–510.
Sneddon, I., 1965. The relation between load and penetration in the axisymmetric Boussinesq problem for a punch of arbitrary profile. Int. J. Eng. Sci. 3, 47–57.
Uchic, M.D., Dimiduk, D.M., 2005. A methodology to investigate size scale effects in crystalline plasticity using uniaxial compression testing. Mater. Sci. Eng. A 400, 268–278.
Uchic, M.D., Dimiduk, D.M., Florando, J.N., Nix, W.D., 2004. Sample dimensions influence strength and crystal plasticity. Science 305, 986–989.
Uchic, M.D., Shade, P.A., Dimiduk, D.M., 2009. Plasticity of micrometer-scale single crystals in compression. Annu. Rev. Mater. Res. 39, 361–386.
Volkert, C.A., Lilleodden, E.T., 2006. Size effects in the deformation of sub-micron Au columns. Philos. Mag. 86, 5567–5579.
Zhang, H., Schuster, B., Wei, Q., Ramesh, K., 2006. The design of accurate micro-compression experiments. Scr. Mater. 54, 181–186.